

Flux-induced strengthening of the magnetic couplings in a flat-band diamond chain

Biplab Pal,^{1,*} Maxime Thumin,^{2,†} and Georges Bouzerar^{3,‡}

¹*Department of Physics, School of Sciences, Nagaland University, Lumami-798627, Nagaland, India*

²*Université Grenoble Alpes, CEA, IRIG-MEM-L SIM, F-38000 Grenoble, France*

³*Université Grenoble Alpes, CNRS, Institut NEEL, F-38042 Grenoble, France*

(Dated: March 2, 2026)

The physics in flat bands has emerged as an essential field in condensed matter physics where a plethora of phenomena can be unveiled, such as anomalous transport properties, superconductivity dominated by quantum geometry or exotic topological phases. Our goal here is to show that even in magnetic systems, the presence of flat bands can give rise to unexpected features. More precisely, we address the impact of an Aharonov-Bohm (AB) flux on the exchange couplings in magnetic diamond chains. The most remarkable result is the significant amplification of magnetic couplings at short distances induced by the AB flux, leading to a considerable increase in the thermal conductivity of the magnons. We have also shown that the flux-dependent decaying length of the couplings is connected to the quantum metric of the flat bands. Our results could be of interest for the control of magnetic properties in spintronic devices and relevant for the heat transport by magnons at the nanoscale in quantum technologies.

I. INTRODUCTION

In recent years, flat band (FB) physics has become one of the most fascinating research topics in physics and in materials science [1–4]. Due to the quenching of the kinetic energy, FBs provide an ideal platform to address a plethora of strongly correlated phenomena, such as ferromagnetism [5–8], superconductivity [9–13], or even the quantum Hall effect [14–16]. The area of physics in flat bands is not limited to an exciting playground for theoreticians; it is also experiencing significant development in experimental research. The interest for FBs does not cease to grow in various directions. FBs are attracting considerable attention in many research areas, including photonic lattices [17–20], Moiré superlattices [2, 21, 22], topo-electrical circuits [23–26] and quantum electrodynamics (QED) lattices as well [27]. Recently, FBs have also been proposed for the realization of quantum storage device [28]. From a technological application perspective, the search for new materials with FBs near the Fermi level is a crucial challenge for material science. Realistic studies of various materials using DFT calculations play an essential role in facilitating this quest [29–32].

In this study, our main objective is to reveal a fascinating physical phenomenon that occurs in magnetic systems with flat bands near the Fermi energy. We demonstrate that in such FB systems, it is possible to boost the magnetic couplings (at short distances) between localized spins by tuning an external magnetic flux. Furthermore, it will also be shown that the flux has a strong impact on the magnon branches and leads to a considerable increase in the thermal conductivity associated to the magnons. To illustrate this interesting phenomenon,

we consider the case of the one-dimensional diamond lattice, also known as the rhombic lattice which consists of two different sublattices Λ (A sites) and Λ' (B and C sites) as depicted in Fig. 1(a). Because of the bipartiteness of the lattice, and since $|\Lambda'| - |\Lambda| = 1$, the diamond chain has a FB at $E = 0$, whose eigenstates have a non-zero weight only on the orbitals of the sublattice Λ' as shown in Fig. 1(b). The classical localized spins are coupled locally to the orbitals of the sublattice Λ' .

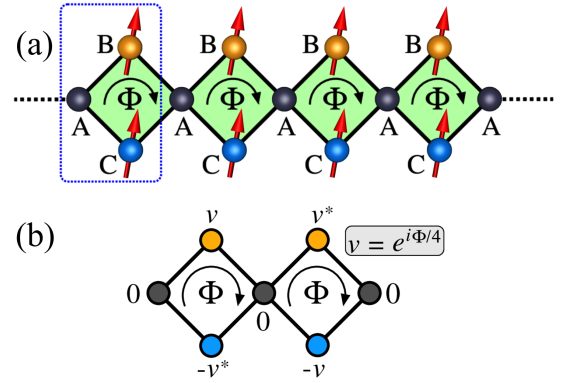


FIG. 1: (a) Representation of the magnetic diamond chain threaded by an external magnetic flux Φ . The red arrows correspond to the localized classical spins located on B and C sites. The boxed area indicates the unit cell. The flux-dependent compact localized state (CLS) is depicted in panel (b). The CLS spreads over two unit cells, and its amplitudes in each site are shown.

Before we discuss the impact of the magnetic flux on the exchange couplings in the magnetic rhombic chains, we briefly recall that the effect of an Aharonov-Bohm (AB) flux [33] in certain types of non-magnetic geometries has been widely studied [34–39]. The reason is that the AB flux leads to an extreme localization phenomenon, known as the AB caging. This localization originates from destructive quantum interferences

*Corresponding author; E-mail: biplab@nagalanduniversity.ac.in

†E-mail: maxime.thumin@cea.fr

‡E-mail: georges.bouzerar@neel.cnrs.fr

of different tunneling pathways. As a result, all dispersive bands of the single-particle spectrum become completely flat [34–36]. The AB caging phenomenon has also been realized in experiments using the femtosecond laser-writing techniques in photonics [40–42], as well as with ultracold atoms in optical lattices [43].

II. HAMILTONIAN AND SPECTRUM

The Hamiltonian that describes electrons in interaction with the localized spins in the magnetic diamond chain threaded by a magnetic flux Φ reads,

$$\hat{H} = \sum_{\langle i\lambda, j\lambda' \rangle, \sigma} \left[t_{ij}^{\lambda\lambda'}(\Phi) \hat{c}_{i\lambda\sigma}^\dagger \hat{c}_{j\lambda'\sigma} + \text{h.c.} \right] + J \sum_{i, \lambda \in \Lambda'} \hat{\mathbf{s}}_{i\lambda} \cdot \mathbf{S}_{i\lambda}. \quad (1)$$

$\hat{c}_{i\lambda\sigma}^\dagger$ creates an electron with spin $\sigma = \uparrow, \downarrow$ in the orbital λ of the i -th cell. $\langle i\lambda, j\lambda' \rangle$ means nearest-neighbors. $t_{ij}^{\lambda\lambda'}(\Phi) = -te^{\pm i\Phi/4}$ depending on whether we go clockwise or anti-clockwise. J is the local coupling between the localized classical spin $\mathbf{S}_{i\lambda} = S\mathbf{e}_{i\lambda}$ at $\mathbf{r}_{i\lambda}$ ($\mathbf{e}_{i\lambda}$ being a unit vector) and that of the itinerant carrier, $\hat{s}_{i\lambda}^p = \hat{c}_{i\lambda\alpha}^\dagger [\hat{\sigma}^p]_{\alpha\beta} \hat{c}_{i\lambda\beta}$ where $p = x, y,$ and z , and $\hat{\sigma}^p$ being the Pauli matrices. In what follows, we set $t = 1$ and JS is expressed in units of t . Here, we focus essentially on the case of half-filled diamond. We define ‘ a ’ as the size of the unit cell (distance between the nearest neighbor orbitals A), and for simplicity, we set $a = 1$.

The lattice being bipartite and the localized spins being located on the same sublattice, at $T = 0$ K, the ground-state is ferromagnetic [8, 44, 45]. Choosing the localized spin orientation along the z -axis, the second term in the Hamiltonian as given in Eq. (1) becomes $\frac{1}{2}z_\sigma JS \sum_{i, \lambda \in \Lambda'} \hat{c}_{i\lambda\sigma}^\dagger \hat{c}_{i\lambda\sigma}$, where $z_\sigma = 1$ for $\sigma = \uparrow$ (resp. $z_\sigma = -1$ for $\sigma = \downarrow$). Here, we consider $J \geq 0$, the case $J \leq 0$ being equivalent. In momentum space, the Hamiltonian is diagonalized separately in the two spin sectors (see Appendix A). The eigen-spectrum reads, $E_\pm^\sigma = \frac{1}{2}[z_\sigma \frac{JS}{2} \pm \sqrt{\Delta_\Phi(k)}]$ and $E_0^\sigma = z_\sigma \frac{JS}{2}$, where $\Delta_\Phi(k) = \frac{1}{4}J^2S^2 + 16t^2[1 + \cos(\frac{\Phi}{2})\cos(k)]$. The flat band survives even in the presence of the magnetic flux and its energy is flux independent. In the basis $(\hat{c}_{kA\sigma}^\dagger, \hat{c}_{kB\sigma}^\dagger, \hat{c}_{kC\sigma}^\dagger)$, its eigenstate is $|\Psi_0^\sigma\rangle = \frac{1}{\sqrt{1 + \cos(\frac{\Phi}{2})\cos(k)}} (0, -\cos(\frac{k}{2} + \frac{\Phi}{4}), \cos(\frac{k}{2} - \frac{\Phi}{4}))$. We remark that, real space FB eigenstates that possess a minimal finite support (non-vanishing weight on a restricted number of sites), known as the compact localized eigenstates (CLS) can be constructed as well. In Fig. 1(b), the CLS which depends on Φ only is depicted; its expression is $|\text{CLS}\rangle_{i, i+1} = \frac{1}{2}[v|B_i\rangle - v^*|C_i\rangle + v^*|B_{i+1}\rangle - v|C_{i+1}\rangle]$, where $v = e^{i\Phi/4}$. We remark that, for a non-zero flux, the CLS spread is over two unit cells, while for $\Phi = 0$, it reduces to a single one.

In Fig. 2, we have depicted the energy dispersions for different values of the flux Φ and a fixed value of the local

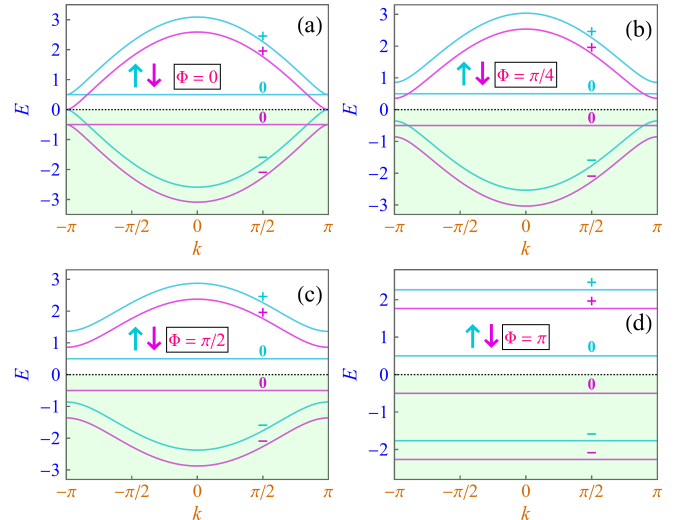


FIG. 2: Energy dispersions in both \uparrow and \downarrow sectors as a function of the momentum (k), for different values of the flux Φ . The labels $+$, $-$, and 0 correspond respectively to the two dispersive bands and to the flat band of each spin sector (see main text). The green area indicates the occupied states. Here, we have chosen $JS = 1$.

coupling $JS = 1$. In what follows, we label the bands (σ, l) where $l = +, -, \text{ and } 0$. In the absence of flux, the bands $(\uparrow, 0)$ and $(\uparrow, +)$ [resp. $(\downarrow, 0)$ and $(\downarrow, -)$] exhibit a quadratic band touching at $|k| = \pi$. In addition, the bands $(\downarrow, +)$ and $(\uparrow, -)$ touch as well quadratically at the zone boundary of the Brillouin zone, which will have an effect on the nature of the couplings as discussed below. When the flux is switched on, in both spin sectors the flat band is now gapped, and a gap opens up between $(\downarrow, +)$ and $(\uparrow, -)$ at $|k| = \pi$. As Φ increases, the width of the dispersive bands reduces till all bands become completely flat when $\Phi = \pi$. As pointed out previously, this is the Aharonov-Bohm caging effect [34–36].

III. EXCHANGE COUPLINGS AND MAGNETIC FORCE THEOREM

To address the nature of the exchange couplings between the magnetic atoms in the flux-threaded magnetic diamond chain, we rely on the magnetic force theorem (MFT) [46–48]. The MFT is a reliable and widely used tool in practical calculations of couplings in real compounds such as transition metals [49], oxides [50], Heusler compounds [51], diluted magnetic semiconductors [52, 53] and even in magnetic molecules [54] to name a few only. Within the MFT, the coupling between two spins located at $r_{i\lambda}$ and $r_{j\lambda'}$ is given by,

$$J_{\lambda\lambda'}(R) = \frac{(JS)^2}{2} \int_{-\infty}^{+\infty} \chi_{ij}^{\lambda\lambda'}(\omega) f(\omega) d\omega, \quad (2)$$

where $R = r_{i\lambda} - r_{j\lambda'}$ and the generalized spin susceptibility $\chi_{ij}^{\lambda\lambda'}(\omega) = -\frac{1}{\pi} \Im \left[G_{ij\uparrow}^{\lambda\lambda'}(\omega) G_{ji\downarrow}^{\lambda'\lambda}(\omega) \right]$. The Green's function $\hat{G}_\sigma(\omega) = (\omega + i\eta - \hat{H}_\sigma)^{-1}$, \hat{H}_σ being the Hamiltonian in the spin sector σ ($\sigma = \uparrow, \downarrow$), η mimics an infinitesimal inelastic scattering rate and $f(\omega) = \frac{1}{e^{(\omega-\mu)/k_B T} + 1}$ is the Fermi-Dirac distribution. Here, we consider half-filled systems at $T = 0$ K ($\mu = 0$).

Eq. (2) is derived for classical spins and implies that the corresponding effective Heisenberg Hamiltonian reads,

$$\mathcal{H}_{Heis} = \frac{1}{2} \sum_{i\lambda \neq j\lambda'} J_{\lambda\lambda'}(r_{ij}^{\lambda\lambda'}) \mathbf{e}_{i\lambda} \cdot \mathbf{e}_{j\lambda'}. \quad (3)$$

This implies that $J_{\lambda\lambda'}(R) \geq 0$ (resp. $J_{\lambda\lambda'}(R) \leq 0$) means antiferromagnetic (resp. ferromagnetic) coupling.

It is very instructive to re-express the couplings in terms of the eigenstates of the Hamiltonian given in Eq.(1), this will be useful for discussing the results of the following section. Eq. (2) can be rewritten in terms of the different inter-band contributions as,

$$J_{\lambda\lambda'}(R) = \sum_{pq} I_{\lambda\lambda'}^{pq}(R), \quad (4)$$

where p (resp. q) is the band index in the \uparrow (resp. \downarrow) spin sector. The inter-band contribution reads,

$$I_{\lambda\lambda'}^{pq}(R) = \frac{(JS)^2}{2N^2} \sum_{k,k'} e^{i(k-k')R} A_{k\lambda,k'\lambda'}^{pq} \times \frac{f(E_p^\uparrow(k)) - f(E_q^\downarrow(k'))}{E_p^\uparrow(k) - E_q^\downarrow(k')}, \quad (5)$$

N is the number of cells, and the inter-band matrix element

$$A_{k\lambda,k'\lambda'}^{pq} = \langle k\lambda\uparrow | \psi_p^\uparrow(k) \rangle \langle \psi_p^\uparrow(k) | k\lambda'\uparrow \rangle \cdot \langle k'\lambda'\downarrow | \psi_q^\downarrow(k') \rangle \langle \psi_q^\downarrow(k') | k'\lambda\downarrow \rangle, \quad (6)$$

where $|k\lambda\sigma\rangle = \hat{c}_{k\lambda\sigma}^\dagger |0\rangle$, $\hat{c}_{k\lambda\sigma}^\dagger$ being the Fourier transform of $\hat{c}_{i\lambda\sigma}^\dagger$. In what follows, we will focus on the AB flux dependence of certain specific contributions, such as the FB-FB contribution $I_{\lambda\lambda'}^{00}(R)$.

IV. IMPACT OF THE MAGNETIC FLUX ON THE (B, B) AND (B, C) COUPLINGS

In this section, we focus primarily on $J_{BB}(R)$, since by symmetry, $J_{CC}(R)$ is identical. Furthermore, we expect as well that $J_{BC}(R) = J_{BB}(R)$ for $R \geq a$. The only difference is the intra-cell coupling $J_{BC}(0)$, which is calculated separately.

In Fig. 3, we have depicted the nearest neighbor (B, B) coupling as a function of JS for the flux Φ ranging from 0 to π . For small values of JS , we observe a rapid monotonic increase of the coupling as the flux increases. For

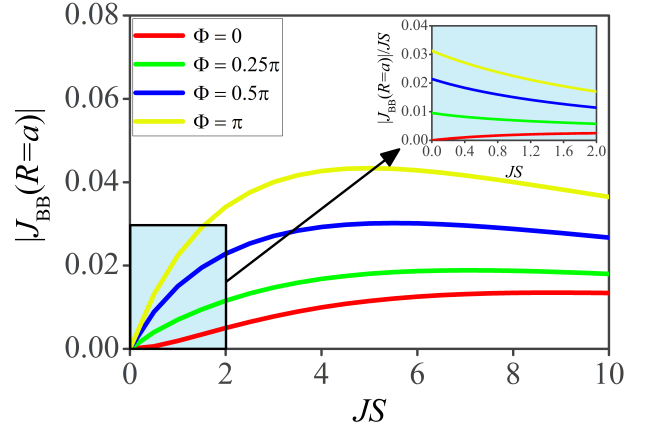


FIG. 3: Amplitude of the nearest neighbor coupling $J_{BB}(R = a)$ as a function of JS for different values of the magnetic flux Φ , as depicted in the figure. The inset shows $J_{BB}(R = a)/JS$ as a function of JS in the weak coupling regime.

instance, for $JS = 1$, the coupling jumps by an order of magnitude, from $J_{BB}(R = a) \sim 0.0025$ for $\Phi = 0$ to $J_{BB}(R = a) \sim 0.02$ for $\Phi = \pi$. In addition, as shown in the inset, $J_{BB}(R = a)$ scales quadratically with JS when $\Phi = 0$ and linearly (with an increasing slope) when $\Phi \neq 0$. As JS increases further, $J_{BB}(R = a)$ continues to increase until it reaches a maximum whose position depends on the flux; for $\Phi = 0$, $(JS)_{\max} \approx 8t$, while for $\Phi = \pi$, $(JS)_{\max} \approx 4t$.

We now propose to shed some light on the change of behavior found in the regime of small JS when a finite flux is introduced. First, we recall that in magnetic systems with FBs, the origin of couplings that vary linearly with $|JS|$ is the FB-FB contribution $I_{\lambda\lambda'}^{00}(R)$ which dominates in the weak coupling regime [8, 55]. We find,

$$I_{BB}^{00}(R) = -\frac{|JS|}{8N^2} \left| \sum_k \left[1 - \frac{\sin(\frac{\Phi}{2}) \sin(ka)}{1 + \cos(\frac{\Phi}{2}) \cos(ka)} \right] e^{ikR} \right|^2. \quad (7)$$

In Appendix A, we provide the analytical expression of $I_{BB}^{00}(R)$. This equation shows that, when $\Phi = 0$ this contribution vanishes and explains the origin of the quadratic scaling found in Fig. 3. We return to this particular case in what follows. We remark that, Eq. (7) is valid for any value of JS , but this does not mean that coupling will diverge as $JS \rightarrow \infty$, this is discussed in what follows. As shown in Appendix A, for $R = a$, one finds $I_{BB}^{00}(R = a) = -\frac{|JS|}{8} \left[\frac{\sin(\Phi/2)}{1 + \sin(\Phi/2)} \right]^2$.

Let us now discuss the special case of π -flux threaded diamond plaquettes. All the bands are flat and the couplings can be straightforwardly calculated analytically (see Appendix B). For this value of Φ , the couplings are restricted to the nearest neighbor only. The individual contributions to the couplings are depicted in Fig. 4. All terms are ferromagnetic (F), except I_{BB}^{+0} and I_{BB}^{0-} which are antiferromagnetic (AF). In the limit of large JS , the AF contributions exactly compensate the I_{BB}^{00}

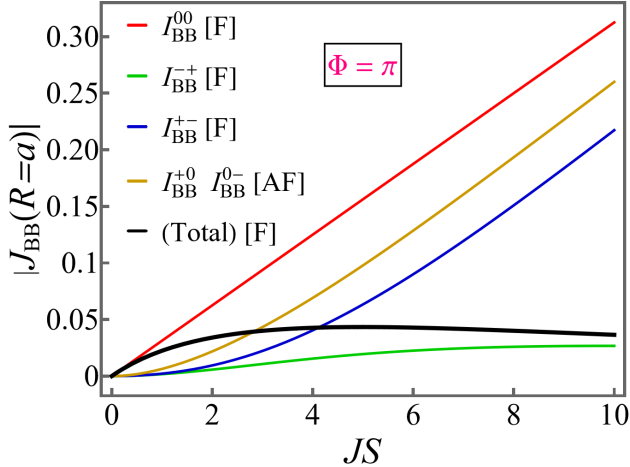


FIG. 4: Amplitude of the nearest neighbor coupling between B sites $J_{BB}(R=a)$ as a function of JS (black line). The other lines correspond to the different contributions as discussed in the main text. ‘[F]’ or ‘[AF]’ means that the contribution is either ferromagnetic or antiferromagnetic. Here we have chosen $\Phi = \pi$.

and I_{BB}^{+-} leading to a $1/JS$ decay of the full coupling and $J_{BB} = I_{BB}^{-+}$ (see Fig. B.1 in Appendix B).

We now propose to discuss the impact of the flux on the decaying length of the magnetic coupling. In Fig. 5(a) and (b), we have plotted $|J_{BB}(R)|$ as a function of the distance R for Φ ranging from 0 to π . We have considered two different values of JS ; $JS = 0.1$ in panel (a) and $JS = 1$ in panel (b). First, qualitatively, we observe a similar behavior; the coupling scales as $e^{-R/\xi(\Phi)}$, where ξ reduces as the flux increases. As pointed out previously, when $\Phi = \pi$, the couplings are restricted to the nearest neighbor only, which means that a fit gives $\xi = 0$. For these values of JS , when $\Phi \neq 0$ the coupling is dominated by the FB-FB term; thus $J_{BB}(R) \approx I_{BB}^{00}(R)$ whose analytical expression is given in Appendix A.

The special case of $\Phi = 0$ was addressed in Ref. [55]. Among the contributions $I_{BB}^{pq}(R)$, only one involves matrix elements between two touching bands: $p = -$ and $q = +$ (see Fig. 2). This is the dominant contribution to $J_{BB}(R)$, which is expected to decrease according to a power law $1/R^\alpha$. In Ref. [55], it was analytically demonstrated that $J_{BB}(R) = -\frac{3t^2}{2\pi|JS|} \frac{1}{R^4}$, which is valid for any value of JS , under the condition that $R \gg \sqrt{32\pi at}/|JS|$.

We now discuss the effect of Φ on the (B, C) coupling and focus on the weak coupling regime. As pointed out above, $J_{BC}(R) = J_{BB}(R)$ for $R \geq a$. However, the intra-cell (B, C) coupling ($R = 0$) requires a separate calculation. In Fig. 6, we have depicted $J_{BC}(0)$ as a function of JS for $\Phi/\pi = 0, 1/4, 1/2$ and 1. First, for a given value of JS , we observe a decrease in $J_{BC}(0)$ as Φ increases, which contrasts with what was found for $J_{BB}(a)$. We remark that, for the specific case of π flux in each plaquette, we find $J_{BC}(0) = 0$ for any value of JS . Secondly,

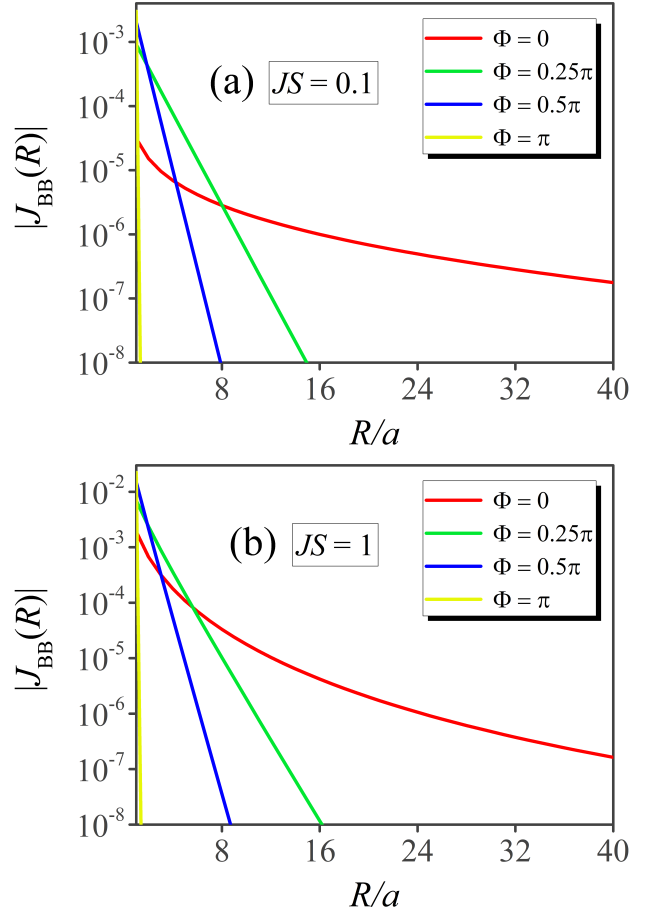


FIG. 5: Coupling $J_{BB}(R)$ as a function of R for (a) $JS = 0.1$ and (b) $JS = 1$. The values of the flux Φ associated to each color are depicted in both the panels.

we find that for any value of Φ the coupling scales linearly with JS even for $\Phi = 0$, which indicates that in the limit of small JS , $J_{BC}(0)$ is dominated by the FB-FB contribution. However, the deviation from the linear behavior increases strongly as the flux approaches to 0, which shows that the other contributions to the coupling rapidly contribute. The expression for the FB-FB contribution can be obtained analytically. One finds,

$$I_{BC}^{00}(0) = -\frac{|JS|}{8} \left[\frac{1 - \sin(\Phi/2)}{1 + \sin(\Phi/2)} \right]. \quad (8)$$

The intra-cell FB-FB contribution decays as the flux increases and vanishes when $\Phi = \pi$.

V. MAGNON SPECTRUM AND MAGNON THERMAL CONDUCTIVITY

In this section, we first discuss how the magnon spectrum is affected by the AB flux. The magnetic system, consisting of two localized spins per unit cell, has two distinct magnon branches: one is optical (gapped mode) and

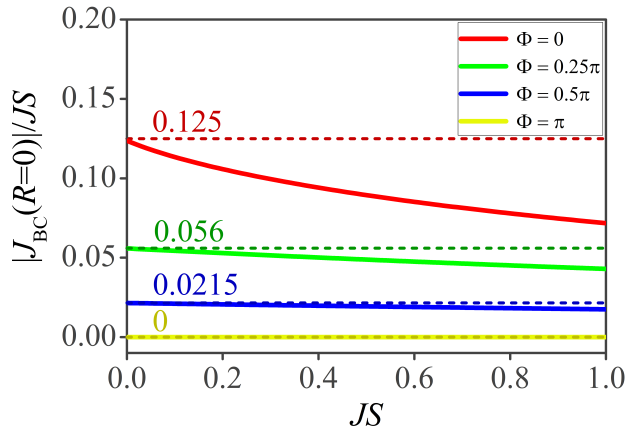


FIG. 6: Rescaled intra-cell BC -coupling $J_{BC}(R=0)$ as a function of JS for different values of the flux Φ . The horizontal dashed lines correspond to the analytical values for $JS \rightarrow 0$, which correspond to the FB-FB contribution $|J_{BC}^{00}(R=0)/JS|$ (see main text).

the other is acoustic (gapless mode). Starting with the Heisenberg Hamiltonian \mathcal{H}_{Heis} as defined in Eq. (3) and following the equation of motion method (RPA decoupling) [56, 57], one finds that the eigenmodes in the magnetic diamond chain are the solution of $\det[D(\omega)] = 0$, where the 2×2 matrix,

$$D(\omega) = \begin{bmatrix} \omega - S f_{BB}(k) & S f_{BC}(k) \\ S f_{CB}(k) & \omega - S f_{CC}(k) \end{bmatrix}, \quad (9)$$

with $f_{BB}(k) = f_{CC}(k) = \bar{J}_{BB}(k) - 2\bar{J}_{BB}(k=0) - J_{BC}(R=0)$ and $f_{BC}(k) = f_{CB}(k) = -\bar{J}_{BB}(k) + J_{BC}(R=0)$, with $\bar{J}_{BB}(k) = \sum_R e^{ikR} J_{BB}(R)$. Note that, we have used the fact that $J_{BB}(R) = J_{CC}(R) = J_{BC}(R)$ for $R \neq 0$. We find two magnon branches, one being dispersive and the second flat: $\omega_{1,2}(k) = S E_{1,2}(k)$ where,

$$E_1(k) = -2 \left[\bar{J}_{BB}(k=0) - \bar{J}_{BB}(k) \right], \quad (10a)$$

$$E_2(k) = -2 \left[\sum_R J_{BB}(R) + J_{BC}(R=0) \right]. \quad (10b)$$

As expected one can check that $E_1(k) = Dk^2$ in the limit of vanishing momentum (Goldstone mode). The impact of the flux on the magnon modes is depicted in Fig. 7(a) and (b) for two different values of JS . In both cases, we observe that as Φ increases the energy of the flat mode reduces. On the other hand, the dispersive mode behaves differently. As Φ is switched on, we find a rapid and strong increase of the magnon bandwidth. The ratio between the bandwidth at $\Phi = \pi$ divided by that at $\Phi = 0$ is approximately 9 for $JS = 1$. It is more impressive when $JS = 0.1$, since the ratio reaches 50. This huge value reflects the fact that in the weak coupling regime the couplings are largely dominated by the FB-FB contribution, as discussed in the previous section.

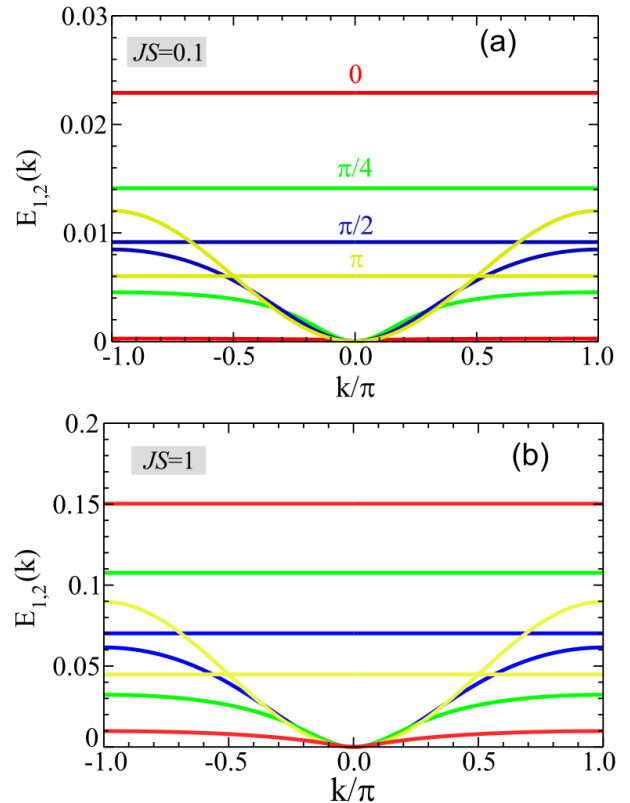


FIG. 7: Magnon modes E_1 (dispersive mode) and E_2 (flat mode) as a function of k for both (a) $JS = 0.1$ and (b) $JS = 1$. The values of the flux Φ which correspond to different colors are depicted in the panel (a).

We now propose to estimate the impact of an AB flux on the thermal transport by magnons. With the spirit of keeping things simple, we consider the constant relaxation time approximation, where the energy and temperature dependence of the magnons is ignored. Similar to the phonon thermal conductivity, that of magnons is given by,

$$\kappa(T) = \frac{1}{2\pi} \int_{-\pi}^{+\pi} dk v^2(k) \omega(k) \tau \frac{\partial f_{BE}}{\partial T}, \quad (11)$$

where $v(k) = \frac{1}{\hbar} \frac{\partial \omega(k)}{\partial k}$ is the magnon velocity, τ is the relaxation time of the magnon mode and $f_{BE} = [e^{\omega(k)/k_B T} - 1]^{-1}$ is the Bose-Einstein distribution. Eq. (11) can be derived following the well-known standard Boltzmann transport equation method.

In Fig. 8, κ is plotted as a function of the temperature T , for $JS = 0.1$ and different values of Φ . First, we immediately see that κ at $\Phi = 0$ is negligible. More precisely, it is about 3 orders of magnitude smaller than that obtained when $\Phi = \pi$. In addition, as the flux varies from $\Phi = \pi/4$ to $\Phi = \pi$, one finds a boost of κ , which increases by about 500% (for $T \geq 0.005 t$). We believe that, these findings could be of interest for energy conversion technologies and nanoscale thermal transport,

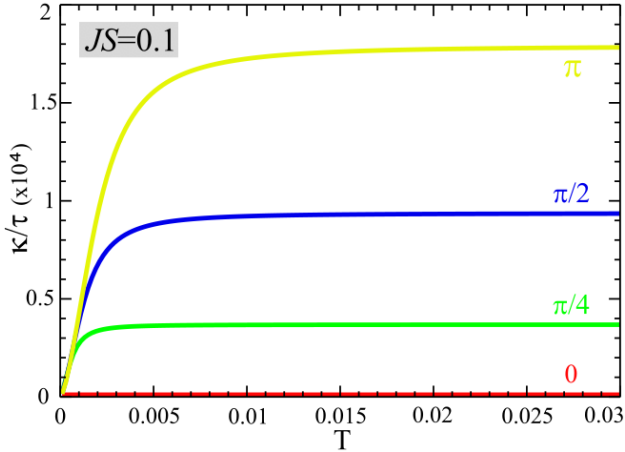


FIG. 8: Magnon thermal conductivity (rescaled) in the constant relaxation time approximation as a function of temperature T (in unit of t). The colors correspond to different values of Φ as in Fig. 7(a). In the case $\Phi = 0$, κ is quasi negligible. Here, we have chosen $JS = 0.1$.

which is relevant for quantum information processing and development of magnonic devices [58–60].

VI. CONNECTION BETWEEN THE DECAYING LENGTH AND THE QUANTUM METRIC

Previously, we have found that for small values of JS and $\Phi \neq 0$, $J_{BB}(R) \approx I_{BB}^{00}(R)$, whose analytical expression is given in Appendix A. In this regime of weak coupling, we can extract the decaying length and find,

$$\xi(\Phi) = \frac{a}{2|\ln z_+|} \quad (12)$$

with $z_+ = \frac{1}{\cos(\Phi/2)} [-1 + \sin(\Phi/2)]$ for $0 < \Phi < \pi$. Thus, when $\Phi \rightarrow 0$ (resp. $\Phi \rightarrow \pi$), the decaying length diverges (resp. vanishes) and $\xi \simeq a/\Phi$ (resp. $\xi \simeq a/4|\ln(\pi - \Phi)|$). In a recent study [55] on dilute magnetic stub chains, it was shown that the characteristic distance over which couplings decay can depend on the quantum metric of the flat band eigenstates in a complex way. We briefly recall that, the quantum metric (QM) corresponds to the real part of the quantum geometric tensor [61–63], while its imaginary part is associated with the Berry curvature. The QM is defined as,

$$g(k) = \langle \partial_k \Psi_k^0 | \partial_k \Psi_k^0 \rangle - |\langle \partial_k \Psi_k^0 | \Psi_k^0 \rangle|^2, \quad (13)$$

where $|\Psi_k^0\rangle$ is the FB eigenstate at $JS = 0$. It should be noted that the average of the QM over the Brillouin zone can be interpreted as a measure of the typical spreading of the FB eigenstates.

It is interesting to compare $\xi(\Phi)$ to the average value of the QM associated to the FB eigenstates. Let us define

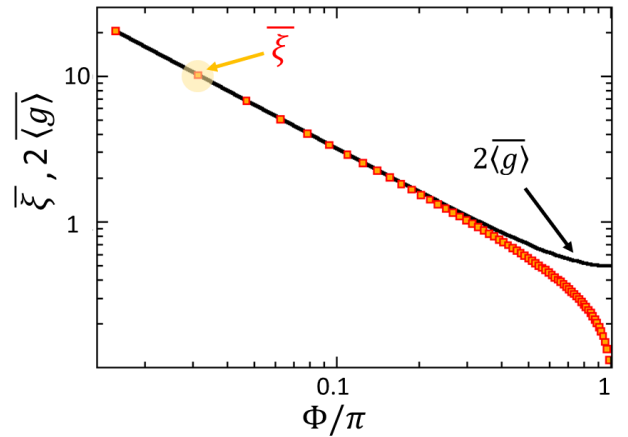


FIG. 9: $\bar{\xi} = \xi(\Phi)/a$ (continuous black line) and $2\overline{\langle g \rangle} = 2\langle g \rangle/a^2$ (square red symbols) as a function of the flux Φ .

$\langle g \rangle = \frac{1}{2\pi} \int_{-\pi}^{+\pi} g(k) dk$, the average value of the QM. Using the expression of the FB eigenstate one finds,

$$g(k) = \frac{a^2 \sin^2(\frac{\Phi}{2})}{4 [1 + \cos(\frac{\Phi}{2}) \cos(ka)]^2}. \quad (14)$$

After performing the integration over the momentum k one obtains,

$$\langle g \rangle = \frac{a^2}{4|\sin(\frac{\Phi}{2})|}. \quad (15)$$

Thus, in the limit of vanishing flux, the QM diverges. This point deserves somehow a small discussion. Indeed, the FB eigenstate at $\Phi = 0$ is momentum independent since the support of its CLS is contained in a single unit cell. This immediately implies that $g(k) = 0$ and hence $\langle g \rangle = 0$, which contradicts Eq. (15). The origin of the conflict is the fact that, at $\Phi = 0$, the QM is not well-defined because of the band touching at $|k| = \pi$ as illustrated in Fig. 2(a).

In Fig. 9, we have depicted the quantum metric and ξ as a function of the flux Φ . An interesting result is revealed – the decaying length coincides with the quantum metric when the flux is small enough. More precisely, when $\Phi \leq 0.3\pi$, we find with a good numerical accuracy that $\xi = 2\langle g \rangle/a$. On the other hand, as the flux Φ approaches the regime of AB caging (*i.e.*, $\Phi = \pi$), we observe that ξ and $\langle g \rangle$ behave differently; while $\xi \rightarrow 0$, the QM saturates, *e.g.*, $\langle g \rangle \rightarrow 1/4$.

VII. ROBUSTNESS AGAINST PERTURBATIONS

So far we have essentially considered the case where the FBs are rigorously flat. However, in real compounds, the hoppings or/and the local couplings will very likely be

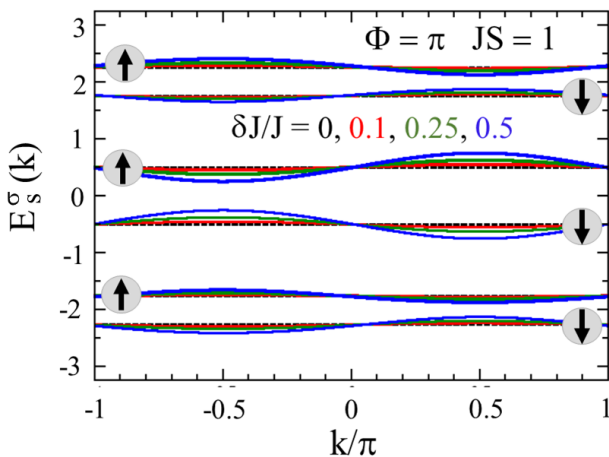


FIG. 10: Energy dispersions E_s^σ as a function of momentum, where $\sigma = \uparrow, \downarrow$ (depicted in the figure) and $s = 0, \pm$ and several values of the ratio $\delta J/J$ corresponding to different colors. Here, we have taken $\Phi = \pi$ and $JS = 1$.

subject to possible perturbations. Hence, it is interesting and relevant to consider in this section the situation, where the flat bands become weakly dispersive. To study how a finite bandwidth of the flat bands affects our findings, we propose to break the equivalence between the way the B and C orbitals are coupled to the localized spins; for this, we replace the second term of the Hamiltonian (1) as follows,

$$J \sum_{i,\lambda \in \Lambda'} \hat{s}_{i\lambda} \cdot \mathbf{S}_{i\lambda} \Rightarrow (J + \delta J) \hat{s}_{iB} \cdot \mathbf{S}_{iB} + (J - \delta J) \hat{s}_{iC} \cdot \mathbf{S}_{iC}. \quad (16)$$

For the sake of clarity, in this section, we consider the case where local coupling $JS = 1$, which will not have an impact on our conclusion. First, as an illustration, in Fig. 10, we have plotted the dispersions for several values of $\delta J/J$ and $\Phi = \pi$. As can be seen, in this case, all the flat bands become dispersive, with a weaker impact in the vicinity of $|k| = 0, \pi$. As expected, the width of the quasi FBs increases almost linearly with δJ .

Fig. 11(a) and (b) represents respectively the (B, B) and (C, C) couplings between nearest-neighbor pairs as a function of the flux for several values of δJ . We consider first $J_{BB}(R = a)$. For small values of Φ , we find a rapid suppression of the ferromagnetic character of the coupling. Indeed, for $\delta J \geq 0.05$, $J_{BB}(R = a)$ becomes antiferromagnetic. In contrast, in the vicinity of $\Phi = \pi$, δJ has the opposite effect since the ferromagnetic coupling is enhanced. On the other hand, $J_{CC}(R = a)$ remains ferromagnetic at small flux and its amplitude increases as δJ is switched on. For a flux $\Phi \approx \pi$, we observe that $J_{CC}(R = a)$ decreases only slightly as δJ increases. More precisely, we find that $\delta J_{CC} = -0.017 \delta J$. Thus, Fig. 11 confirms that the strong increase in the couplings induced by the AB flux seems to be robust against the perturbations which make the FBs weakly dispersive.

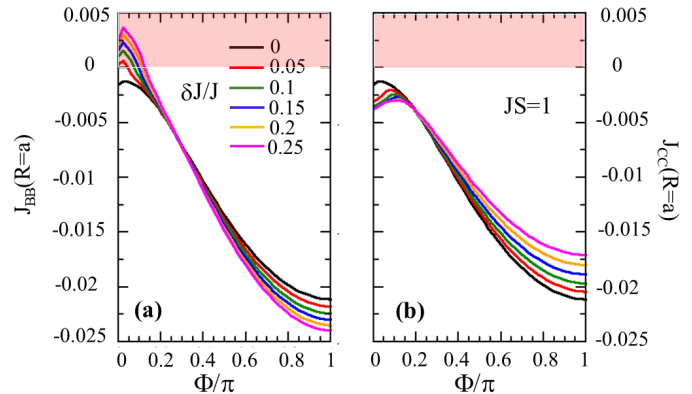


FIG. 11: (a) $J_{BB}(R = a)$ and (b) $J_{CC}(R = a)$ as a function of Φ for different values of δJ and $JS = 1$ (see main text). The red area corresponds to antiferromagnetic couplings.

VIII. CONCLUSIONS

In conclusion, this work has shown that exchange couplings at short distances in the magnetic diamond chain can be strongly amplified in the presence of an AB flux and also lead to a giant increase in the magnon thermal conductivity. The effect is particularly pronounced when the local coupling between the itinerant carrier and the localized spins is weak. It is also revealed that, this phenomenon is robust against perturbations that would make the flat bands weakly dispersive. We have established a connection between the flux-dependent decaying length of the couplings and the quantum metric of the flat bands. Although, the present study focused only on the case of the diamond chain, our results are general and can be applied to other geometries and lattices exhibiting flat bands in the vicinity of the half-filled system. We believe that our results could be of interest for both spintronics and magnonics.

Acknowledgments

BP gratefully acknowledges the local hospitality and the funding provided by the CNRS during his research visit to the Néel Institute, where this work was initiated. BP would also like to thank the Nagaland University for providing a minor start-up research grant.

Appendix A: Flux dependence of the FB-FB contribution to the (B, B) coupling

In this appendix, we propose to derive the analytical expression of I_{BB}^{00} , the FB-FB contribution to the (B, B) coupling. Assuming a ferromagnetic spin texture for the localized spins, in the basis $(\hat{c}_{kA\sigma}^\dagger, \hat{c}_{kB\sigma}^\dagger, \hat{c}_{kC\sigma}^\dagger)$ in k space, the Hamiltonian given in equation Eq. (1) becomes,

$$\hat{H} = \begin{bmatrix} \hat{h}_\uparrow & 0_{3 \times 3} \\ 0_{3 \times 3} & \hat{h}_\downarrow \end{bmatrix}, \quad (A1)$$

where,

$$\hat{h}_\sigma = \begin{bmatrix} 0 & f_+ & f_- \\ f_+ & \epsilon_\sigma & 0 \\ f_- & 0 & \epsilon_\sigma \end{bmatrix}, \quad (\text{A2})$$

with $f_\pm = -2t \cos(k/2 \pm \Phi/4)$, $\epsilon_\sigma = z_\sigma \frac{JS}{2}$ and $z_\sigma = \pm 1$ for $\sigma = \uparrow, \downarrow$. In each spin sector, the energy spectrum reads, $E_\pm^\sigma = \frac{1}{2} [z_\sigma \frac{JS}{2} \pm \sqrt{\Delta_\Phi(k)}]$ and $E_0^\sigma = z_\sigma \frac{JS}{2}$ where $\Delta_\Phi(k) = \frac{1}{4} J^2 S^2 + 16t^2 [1 + \cos(\frac{\Phi}{2}) \cos(k)]$. The corresponding eigenvectors are $|\Psi_\pm^\sigma\rangle = \frac{1}{\sqrt{N_\pm^\sigma}} (E_\pm^\sigma - z_\sigma \frac{JS}{2}, -f_-, -f_+)$, where $N_\pm^\sigma = 4t^2 [1 + \cos(\frac{\Phi}{2}) \cos(k)] + [E_\pm^\sigma - z_\sigma \frac{JS}{2}]^2$. The FB eigenstate has the same expression in both spin sectors and is given by $|\Psi_0^\sigma\rangle = \frac{1}{\sqrt{1 + \cos(\frac{\Phi}{2}) \cos(k)}} (0, f_+/2, -f_-/2)$.

The FB-FB contribution to the (B, B) coupling is given by,

$$I_{BB}^{00}(R) = \frac{(JS)^2}{2N^2} \sum_{k, k'} e^{i(k-k')R} A_{kB, k'B}^{00} \times \frac{f(E_0^\uparrow(k)) - f(E_0^\downarrow(k'))}{E_0^\uparrow(k) - E_0^\downarrow(k')}, \quad (\text{A3})$$

with $A_{kB, k'B}^{00} = |\langle kB | \Psi_0^\uparrow \rangle|^2 \times |\langle k'B | \Psi_0^\downarrow \rangle|^2$. This becomes

$$I_{BB}^{00}(R) = -\frac{|JS|}{2} |F_\Phi^{BB}(R)|^2, \quad (\text{A4})$$

where for simplicity, we have introduced $F_\Phi^{BB}(R) = \frac{1}{N} \sum_k e^{ikR} \frac{\cos^2(k/2 + \Phi/4)}{[1 + \cos(\Phi/2) \cos(k)]}$. It can be re-written as,

$$F_\Phi^{BB}(R) = \frac{\sin(\Phi/2)}{4\pi} \oint_{C_1} \frac{(z^2 - 1)z^{n-1}}{f_\Phi(z)} dz, \quad (\text{A5})$$

where $f_\Phi(z) = \cos(\Phi/2)z^2 + 2z + \cos(\Phi/2)$ and C_1 is the unit circle, $R = na$ and $n \geq 1$. To calculate $F_\Phi^{BB}(R)$, we perform a standard residue calculation for simple poles.

The flux dependent poles are $z_\pm = \frac{1}{\cos(\Phi/2)} [-1 \pm \sin(\Phi/2)]$ where, for $0 \leq \Phi \leq \pi$, z^+ (resp. z^-) is inside (resp. outside) the contour. Thus we find,

$$I_{BB}^{00}(R) = -\frac{|JS|}{8|z_+|^2} \frac{\sin^2(\Phi/2)}{[1 + \sin(\Phi/2)]^2} e^{-\frac{R \ln |z_+|^{-2}}{a}}. \quad (\text{A6})$$

Thus, the decaying length $\xi(\Phi)$ is given by,

$$\xi(\Phi) = \frac{a}{2 |\ln |z_+||}. \quad (\text{A7})$$

Appendix B: $J_{BB}(R)$ for $\Phi = \pi$ as a function of JS

As discussed in the main text of the manuscript, for the special case of $\Phi = \pi$, all the bands are dispersionless

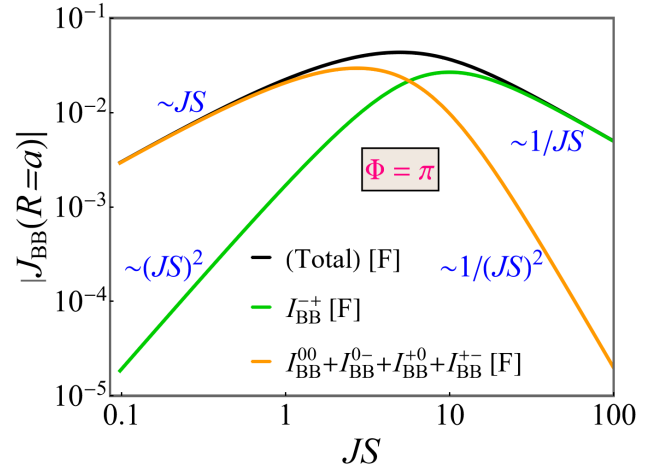


FIG. B.1: $|J_{BB}(R = a)|$ and its contributions as a function of JS for $\Phi = \pi$. $|J_{BB}(R = a)|$ corresponds to the black line, $|I_{BB}^{-+}|$ is plotted in green and the sum of the other contributions $|I_{BB}^{00} + I_{BB}^{0-} + I_{BB}^{+0} + I_{BB}^{+-}|$ appears in orange. ‘[F]’ means that the coupling is ferromagnetic. The scaling in the weak and strong coupling regime is depicted as well.

which allows for the analytical calculation of the couplings and its different contributions. Note that in this appendix, we use the same notations as those defined in the main text and in Appendix A.

In Fig. B.1, we have depicted $|J_{BB}(R = a)|$ as a function of JS . As discussed in the main text, the coupling (B, B) is dominated by the FB-FB contribution (I_{BB}^{00}) when $JS \leq 1$, while it is controlled by the single contribution I_{BB}^{-+} when $JS \gg 1$. We now propose to give the analytical expression of I_{BB}^{00} and I_{BB}^{-+} . Using the expression of the eigenvalues and eigenvectors as given in the Appendix A, one finds,

$$I_{BB}^{00}(R) = -\frac{|JS|}{32} \delta_{|R|, a}. \quad (\text{B1})$$

Similarly, we find,

$$I_{BB}^{-+}(R) = -\frac{(JS)^2}{8(\Delta - \frac{JS}{2}) [1 + (\frac{\Delta}{2t} + \frac{JS}{4t})^2]^2} \delta_{|R|, a}. \quad (\text{B2})$$

where we have introduced $\Delta = \sqrt{\frac{J^2 S^2}{4} + 16t^2}$.

These two expressions indicate that the couplings reduce to nearest neighbor only, which could have been anticipated. It is as well the case for the other missing contributions.

In the limit of large values of JS , Eq. (B2) leads to,

$$I_{BB}^{-+}(R) = -\frac{t^2}{8|JS|} \delta_{|R|, a}, \quad (\text{B3})$$

which explains the scaling of $J_{BB}(R = a)$ in the large coupling regime as depicted in Fig. B.1.

-
- [1] D. Leykam, A. Andreanov, and S. Flach, *Adv. Phys. X* **3**, 1473052 (2018).
- [2] L. Balents, C. R. Dean, D. K. Efetov, and A. F. Young, *Nat. Phys.* **16**, 725 (2020).
- [3] L. Tang, D. Song, S. Xia, S. Xia, J. Ma, W. Yan, Y. Hu, J. Xu, D. Leykam, and Z. Chen, *Nanophotonics* **9**, 1161 (2020).
- [4] R. A. Vicencio Poblete, *Adv. Phys. X* **6**, 1878057 (2021).
- [5] A. Mielke, *J. Phys. A Math. Gen.* **24**, L73 (1991).
- [6] H. Tasaki, *Phys. Rev. Lett.* **69**, 1608 (1992).
- [7] M. Maksymenko, A. Honecker, R. Moessner, J. Richter, and O. Derzhko, *Phys. Rev. Lett.* **109**, 096404 (2012).
- [8] G. Bouzerar, *Phys. Rev. B* **107**, 184441 (2023).
- [9] S. Peotta and P. Törmä *Nat. Commun.* **6**, 8944 (2015).
- [10] V. J. Kaupilla, F. Aikebaier, and T. T. Heikkilä, *Phys. Rev. B* **93**, 214505 (2016).
- [11] H. Aoki, *J. Supercond. Nov. Magn.* **33**, 2341 (2020).
- [12] L. H. C. M. Nunes and C. M. Smith, *Phys. Rev. B* **101**, 224514 (2020).
- [13] G. Bouzerar and M. Thumin, *Phys. Rev. B* **107**, 214508 (2023).
- [14] E. Tang, J.-W. Mei, and X.-G. Wen, *Phys. Rev. Lett.* **106**, 236802 (2011).
- [15] K. Sun, Z. Gu, H. Katsura, and S. Das Sarma, *Phys. Rev. Lett.* **106**, 236803 (2011).
- [16] T. Neupert, L. Santos, C. Chamon, and C. Mudry, *Phys. Rev. Lett.* **106**, 236804 (2011).
- [17] R. A. Vicencio, C. Cantillano, L. Morales-Inostroza, B. Real, C. Mejía-Cortés, S. Weimann, A. Szameit, and M. I. Molina, *Phys. Rev. Lett.* **114**, 245503 (2015).
- [18] S. Mukherjee, A. Spracklen, D. Choudhury, N. Goldman, P. Öhberg, E. Andersson, and R. R. Thomson, *Phys. Rev. Lett.* **114**, 245504 (2015).
- [19] S. Longhi, *Opt. Lett.* **39**, 5892 (2014).
- [20] S. Xia, Y. Hu., D. Song, Y. Zong, L. Tang, and Z. Chen, *Opt. Lett.* **41**, 1435 (2016).
- [21] Z. Zhang, Y. Wang, K. Watanabe, T. Taniguchi, K. Ueno, E. Tutuc, and B. J. LeRoy, *Nat. Phys.* **16**, 1093 (2020).
- [22] H. Li *et al.*, *Nat. Mater.* **20**, 945 (2021).
- [23] H. Wang, W. Zhang, H. Sun, and X. Zhang, *Phys. Rev. B* **106**, 104203 (2022).
- [24] X. Zhou, W. Zhang, H. Sun, and X. Zhang, *Phys. Rev. B* **107**, 035152 (2023).
- [25] W. Zhang, H. Wang, H. Sun, and X. Zhang, *Phys. Rev. Lett.* **130**, 206401 (2023).
- [26] C. Chase-Mayoral, L. Q. English, N. Lape, Y. Kim, S. Lee, A. Andreanov, S. Flach, and P. G. Kevrekidis, *Phys. Rev. B* **109**, 075430 (2024).
- [27] A. J. Kollár, M. Fitzpatrick, P. Sarnak, and A. A. Houck *Commun. Math. Phys.* **376**, 1909 (2020).
- [28] C. Danieli, J. Liu, R. A. Römer, and R. A. Vicencio, *arXiv:2508.01846v1*, to appear in *Phys. Rev. Lett.* (2026).
- [29] W. Jiang, Z. Liu, J.-W. Mei, B. Cui, and F. Liu, *Nanoscale* **11**, 955 (2019).
- [30] S. Zhang, M. Kang, H. Huang, W. Jiang, X. Ni, L. Kang, S. Zhang, H. Xu, Z. Liu, and F. Liu, *Phys. Rev. B* **99**, 100404(R) (2019).
- [31] W. Jiang, H. Huang, and F. Liu, *Nat. Commun.* **10**, 2207 (2019).
- [32] N. Regnault *et al.*, *Nature* **603**, 824 (2022).
- [33] Y. Aharonov and D. Bohm, *Phys. Rev.* **115**, 485 (1959).
- [34] J. Vidal, B. Douçot, R. Mosseri, and P. Butaud, *Phys. Rev. Lett.* **85**, 3906 (2000).
- [35] J. Vidal, R. Mosseri, and B. Douçot, *Phys. Rev. Lett.* **81**, 5888 (1998).
- [36] A. Mukherjee, A. Nandy, S. Sil, and A. Chakrabarti, *J. Phys.: Condens. Matter* **33**, 035502 (2021).
- [37] B. Pal, *Phys. Rev. B* **98**, 245116 (2018).
- [38] B. Pal and G. Bouzerar, *J. Phys.: Condens. Matter* **37**, 135503 (2025).
- [39] B. Pal, *Phys. Status Solidi RRL* **19**, 2500129 (2025).
- [40] S. Mukherjee, M. Di Liberto, P. Öhberg, R. R. Thomson, and N. Goldman, *Phys. Rev. Lett.* **121**, 075502 (2018).
- [41] G. Cáceres-Aravena, D. Guzmán-Silva, I. Salinas, and R. A. Vicencio, *Phys. Rev. Lett.* **128**, 256602 (2022).
- [42] M. Kremer, I. Petrides, E. Meyer, M. Heinrich, O. Zilberberg, and A. Szameit, *Nat. Commun.* **11**, 907 (2020).
- [43] H. Li, Z. Dong, S. Longhi, Q. Liang, D. Xie, and B. Yan, *Phys. Rev. Lett.* **129**, 220403 (2022).
- [44] E. Lieb, *Phys. Rev. Lett.* **62**, 1201 (1989).
- [45] S. Saremi, *Phys. Rev. B* **76**, 184430 (2007).
- [46] A. I. Liechtenstein, M. I. Katsnelson, and V. A. Gubanov, *J. Phys. F: Met. Phys.* **14**, L125 (1984).
- [47] A. I. Liechtenstein, M. I. Katsnelson, and V. A. Gubanov, *Solid State Commun.* **54**, 327 (1985).
- [48] I. V. Solov'yev, *Phys. Rev. B* **103**, 104428 (2021).
- [49] M. Pajda, J. Kudrnovský, I. Turek, V. Drchal, and P. Bruno, *Phys. Rev. B* **64**, 174402 (2001).
- [50] F. Máca, J. Kudrnovský, V. Drchal, and G. Bouzerar, *Appl. Phys. Lett.* **92**, 212503 (2008).
- [51] Y. Kurtulus, R. Dronskowski, G. D. Samolyuk, and V. P. Antropov, *Phys. Rev. B* **71**, 014425 (2005).
- [52] K. Sato *et al.*, *Rev. Mod. Phys.* **82**, 1633 (2010).
- [53] R. Bouzerar and G. Bouzerar, *Europhys. Lett.* **92**, 47006 (2010).
- [54] V. V. Mazurenko, Y. O. Kvashnin, F. Jin, H. A. De Raedt, A. I. Liechtenstein, and M. I. Katsnelson, *Phys. Rev. B* **89**, 214422 (2014).
- [55] G. Bouzerar and M. Thumin, *SciPost Phys.* **19**, 011 (2025).
- [56] S. V. Tyablicov, *Methods in quantum theory of magnetism* (Plenum Press, New York, 1967).
- [57] G. Bouzerar and P. Bruno, *Phys. Rev. B* **66**, 014410 (2002).
- [58] K. I. Uchida and R. Iguchi, *J. Phys. Soc. Jpn.* **90**, 122001 (2021).
- [59] P. Pirro, V.I. Vasyuchka, A.A. Serga, *et al.*, *Nat. Rev. Mater.* **6**, 1114 (2021).
- [60] K. Baumgaertl, and D. Grundler, *Nat. Commun.* **14**, 1490 (2023).
- [61] J. P. Provost and G. Vallee, *Commun. Math. Phys.* **76**, 289 (1980).
- [62] R. Resta, *Eur. Phys. J. B* **79**, 121 (2011).
- [63] N. Marzari and D. Vanderbilt, *Phys. Rev. B* **56**, 12847 (1997).